Dwivedi and Chandrasekhar
Earth, Planets and Space (2024) 76:61
https://doi.org/10.1186/s40623-024-01996-8

Earth, Planets and Space

FULL PAPER

Open Access

Geomagnetic field variations due to solar tides at the Indian Observatories

Divyanshu Dwivedi[1*] and N. Phani Chandrasekhar[1]

Abstract

This study investigates the response of solar (S) tidal signatures on the horizontal component of the geomagnetic field at two observatories in India during 1980–2002 over solar cycles (SC) 21–23: Hyderabad (HYB), located in the low-latitude region, and Ettaiyapuram (ETT), situated at the magnetic equator. HYB represents the characteristics of solar quiet (Sq), while ETT is under the equatorial electrojet (EEJ) effect. Our results show the additional information about ter (S3), and quarta-diurnal (S4) tidal signatures of Sq and EEJ, along with diurnal (S1) and semi-diurnal (S2) at both observatories. In Sq solar tide, the average amplitude of S1 tide is consistently higher than that of EEJ tide by ~ 10%. During the same period, the S2, S3, and S4 tidal signatures of Sq are weaker than EEJ by ~ 2%, 5%, and 2.5%, respectively. During solar cycle maxima, the amplitude of the Sq tide is higher in SC-21 than in SC-22 and SC-23 by ~ 13% and 16%, while SC-22 has higher EEJ tidal amplitudes than other SCs by ~ 9%. We observe that the tidal signatures of Sq and EEJ closely follow the trend of solar radio flux ($\sqrt{F10.7}$), except for S4 of Sq. The Pearson correlation coefficients (P) between $\sqrt{F10.7}$ and Sq/EEJ tidal amplitudes exhibit negative to positive correlation coefficients during different phases of SCs. The solar tidal amplitudes of Sq/EEJ (S1-S4) with $\sqrt{F10.7}$ during D, E, and J seasons have varying correlation coefficients, indicating that each tide has a distinct response on the geomagnetic field.

Key Points

- During SC-21, stronger amplitudes of Sq solar tides are observed, for EEJ it is SC-22.
- The weak correlation between tidal amplitude and $\sqrt{F10.7}$ may be related to the high occurrence rate of CEJs.
- Except S4 of Sq tide, the remaining tidal amplitudes of Sq and EEJ follow the trend of $\sqrt{F10.7}$.

Keywords Solar tides, Geomagnetic data, Equatorial electrojet, Solar quiet, Seasonal characteristics and solar cycles

*Correspondence:
Divyanshu Dwivedi
ddwivedigp@gmail.com
Full list of author information is available at the end of the article

Graphical Abstract

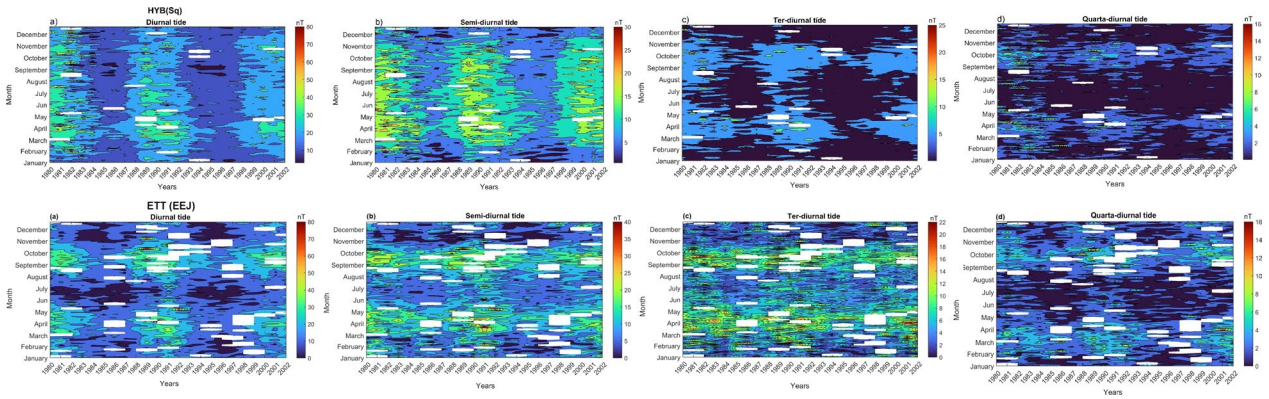

Introduction

The solar-quiet (Sq) is the ionospheric current system occurring in magnetically quiet times. The deviations in Sq are usually understood in terms of neutral wind, plasma density, and the geomagnetic field in the dynamo region. The driving winds for the ionospheric currents that cause Sq variations are solar (S) tides produced nearby in the thermosphere by solar ultraviolet heating (Stening 1969; Tarpley 1970; Takeda and Maeda 1980). The diurnal solar tide (above 150 km) and semi-diurnal solar tides (above 120 km) in the atmosphere are dominant drivers for the Sq current pattern (Garces et al. 2002; Gurubaran et al. 2016 and references therein), which result in day-to-day variability in the geomagnetic field. Apart from Sq, the magnitude of the daily variation in the horizontal component (H) of the geomagnetic field is approximately twofold to threefold increase at the dip equator (± 3°) is caused by a current in the E region of the ionosphere towards an eastward direction, known as equatorial Electrojet (EEJ) during quiet days (Chapman 1951). The large magnitude of the H component at the dip equator occurs due to the EEJ (Onwumechili 1967). The reverse phenomena of EEJ are known as counter electrojet (CEJ), wherein the currents flow in a westward direction and result in depressions in the daily variation below the night-time values (Gouin and Mayaud 1967).

Solar tidal winds at E-region heights can drive sufficiently strong ionospheric currents to explain Sq variation on the ground [e.g., Richmond et al. 1976 and references therein]. The main cause of the solar tidal motion in the upper atmosphere is in-situ heating due to extreme ultraviolet solar radiation absorption by O, O_2, and N_2 on the dayside (Hagan et al. 2001). Solar tides typically have periods of 24 h (hours), 12 h, 8 h, and 6 h. These tides are referred as diurnal tides (S1), semi-diurnal tides (S2), ter-diurnal tides (S3), and quarta-diurnal tides (S4) (Lindzen and Chapman 1969). S1 and S2 have the largest amplitude in the Mesosphere-Lower Thermosphere (MLT). The S2 has large amplitudes near ± 60° N/S but small amplitudes at low latitudes. In contrast, the S1 has large amplitudes at low latitudes but much smaller amplitudes at the middle and high latitudes (Mitchell et al. 2002 and references therein).

Solar migrating tides are primarily induced by the absorption of solar radiation in the troposphere and stratosphere, respectively, by water vapour and ozone (Oberheide and Gusev 2002). These tides move westward with the motion of the Sun and do not cause longitude variability at a given local time across a constant latitude circle. Non-migrating solar tides are not stimulated by solar radiation and do not move in relation to the Sun. As a consequence of this, if observed at a constant local time, they will induce longitudinal fluctuations in the system consisting of the ionosphere and the thermosphere. The majority of the time, non-migrating tides are caused by zonal asymmetries of driving mechanisms (Forbes et al. 2003), nonlinear interactions between the migrating diurnal tide and planetary waves (Hagan et al. 2001), gravity waves (McLandress and Ward 1994), or by the latent heat release in the troposphere (Hagan and Forbes 2003).

The following studies reported solar tidal signatures and their seasonal characteristics at different longitude sectors during different solar cycles using ground, satellite and modelled data sets:

- Rastogi and Iyer (1976) identified the solar cycle dependence is less noticeable for semi-diurnal tides and, even less for ter-diurnal tides, and negligible for quatra-diurnal tides observed in Indian, African and South American sectors.
- Celik et al. (2012) suggested that the amplitudes of the solar harmonics increase from winter to summer and show a good sunspot dependence in the Southeast Europe sector.
- Yamazaki and Kosch (2014) reported that the semi-diurnal component of solar tides correlates with F10.7 and follows a prominent 11-year cycle from eight mid-latitude stations within ± 60° latitude.
- Siddiqui et al. (2018a, b) showed the response of sudden stratospheric warming (SSW) on the EEJ semi-diurnal lunar tides in the South American sector using SABER temperature data and, Whole Atmosphere Community Climate Model (WACCM-X) simulations.
- Using long-term meteor radar wind observations from Brazil, Guharay et al. (2019), found that seasonal profiles of the diurnal and semi-diurnal tidal amplitudes exhibit a prominent relationship with the solar flux during equinoxes.
- Soares et al. (2022) proposed the PCEEJ model to determine the tidal signatures (migrating and non-migrating) in the EEJ and their relations to tides in atmospheric temperature observed by SABER data. This study estimated the S1 and S2 migrating tides with a decreasing trend from 2015 to 2018 related to the solar cycle.
- Sun et al. (2022) estimated the correlations between the migrating and non-migrating tides and solar cycle in the MLT regions using the WACCM-X model. They found negative correlations between tides and F10.7. Further, the tidal amplitudes are larger in solar minimum conditions than solar maximum.

A comprehensive study has yet to be conducted to assess the response of solar tidal signatures during various phases of solar cycles using ground magnetic data from two observatories, one located at the equator and the other at the low-latitude for the solar cycles 21–23. These cycles exhibit a decrease in F10.7 intensity compared to different solar cycles, with cycle 21 having the highest intensity and cycle 23 having the lowest. It has not been determined whether the characteristics of solar cycles 21–23 are similar or distinct. A similar pattern of the descending phase of the solar cycle was observed during 1755–1804 (SC: 3–5) and 1833–1912 (SC: 8–10), but no observations have been made so far. Further, these studies did not extensively discuss about the ter and quarta solar tidal signatures or their relationship with the ascending/descending phases of solar cycles at equatorial and low-latitude observatories. Moreover, these studies discussed the solar tidal signatures and their solar cycle dependence with data sampled at 70-day, annual mean, and 5-year average amplitude variations.

Given that each solar cycle has unique characteristics, it is crucial to comprehend the specifics of each SC phase about the solar tidal signatures and their response to geomagnetic field variations. Therefore, in the present work, by utilizing the geomagnetic horizontal (H) component data from low-latitude Hyderabad (HYB) and equatorial Ettaiyapuram (ETT) geomagnetic observatories, we would like to investigate the following:

i) Characteristics of solar cycles 21, 22, and 23 and their response to geomagnetic field variability by looking into solar tides.
ii) Variability of solar tidal amplitudes (S1, S2, S3, and S4) of the Sq and EEJ during different Lloyd's seasons.
iii) Correlation between the Sq and EEJ solar tides with $\sqrt{F10.7}$ during different phases of solar cycles.
iv) Periodicities of Sq and EEJ with $\sqrt{F10.7}$ over solar cycles 21–23.
v) Coherence and deviations between the ground-derived EEJ signature and the climatological EEJM-2.0 at ETT.
vi) Missing information on S3 and S4 solar tides of Sq and EEJ.

Data and methodology

The hourly mean values of the horizontal (H) component of the geomagnetic field data at equatorial observatory, Ettaiyapuram (ETT), Geographic: 09° 10′N; 78° 01′E; Geomagnetic: 0° 6′S; 147° 5′E; dip: 0.31°), and low-latitude observatory, Hyderabad (HYB, Geographic: 17° 25′N; 78° 33′E; Geomagnetic: 07° 6′N; 148° 9′E; dip: 10.83°) of CSIR-NGRI for the period 1980 to 2002 have been used in the analysis (Fig. 1). The hourly variations in the H component data are calculated by subtracting the mean of local midnight [22:00–02:00 LT] values for each day from the entire dataset.

The EEJ strength is calculated as follows:

$$\Delta H_{EEJ} = \Delta H_{ETT} - \Delta H_{HYB} \quad (1)$$

where ΔH_{EEJ} is the EEJ variation, ΔH_{ETT} and ΔH_{HYB} are the variations of the horizontal component for the ETT (Sq + EEJ) and HYB (Sq) observatories after subtracting the local midnight mean from each day data. This procedure eliminates the Sq part from ETT data (Chandrasekhar et al. 2014; 2017).

The total number of 201600 hourly mean data points for 23 years are used for the ETT and HYB observatories

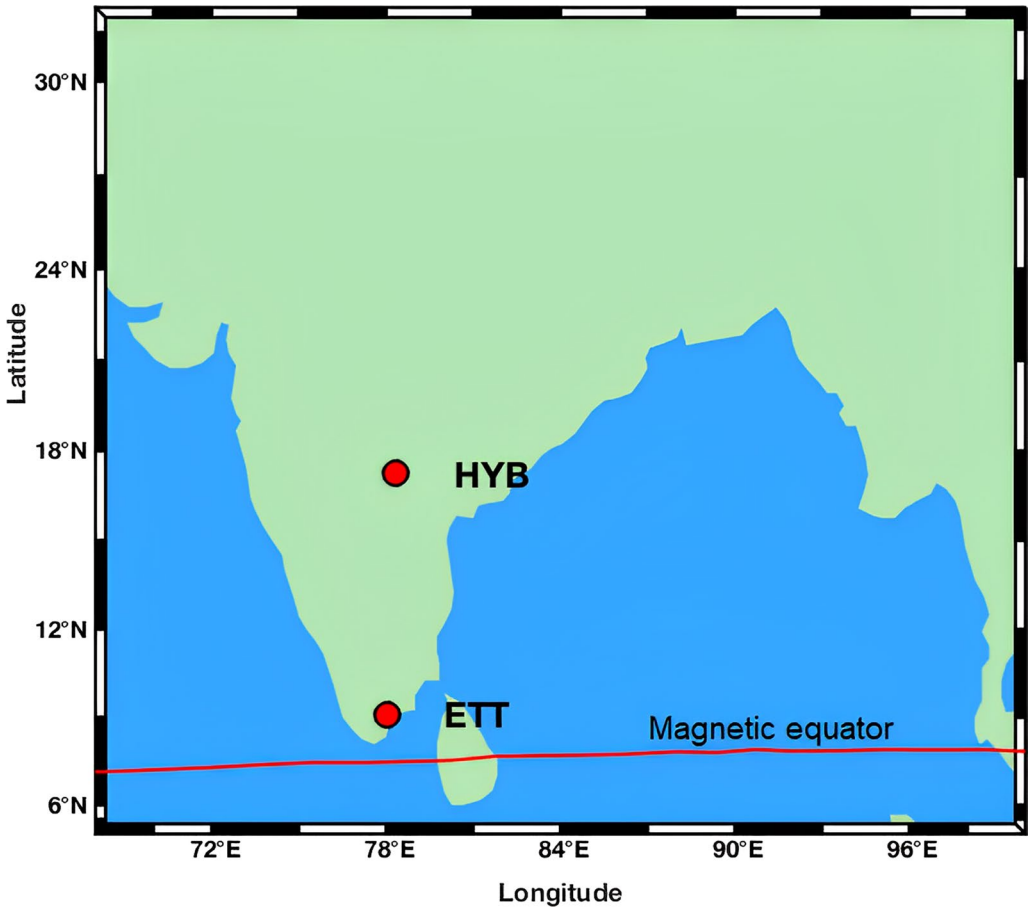

Fig. 1 Location of ETT and HYB magnetic observatories and the redline shows the magnetic equator

of the Council of Scientific and Industrial Research (CSIR)—National Geophysical Research Institute (NGRI), India. Historical data of ETT and HYB have been archived from digital records of WDC-IIG, and missing digital data for a few hours or days were manually entered from the hard copies of Indian Magnetic Data (IMD) volumes. Initially, we plotted the raw data of each observatory separately and compared the trends for the 23 years of data, and confirmed the data quality. After that, we performed the linear interpolation technique on both datasets when the loss of record is not more than five hours at each observatory. We avoided this technique for hours more than the above condition. Hourly mean data of the H component for each month are combined to generate the time series datasets of entire years. The details of data gaps for the observatories are discussed in Text (s1). The hourly mean variations of the ETT and HYB for the 1980–2002 period are shown in Additional file 1: Figure S1.

The hourly mean square root of solar radio emission at 10.7 cm (F10.7) is used as a substitution for solar EUV radiation (https://omniweb.gsfc.nasa.gov/form/dx1.html), which creates ionospheric plasma. In this study, we have used $\sqrt{F10.7}$ in place of F10.7 due to a strong correlation with solar diurnal amplitude (Yamazaki and Kosch 2014). Since the present work aims to study the solar tidal signatures, we have used the revised Dst index (Love and Gannon 2009), which is independent of solar and lunar tides (http://geomag.usgs.gov/products/downloads.php) and also enables us to work on a quiet time part of ΔH variations after removing the disturbance fields during the disturbed days. In general, EEJ and Sq are mostly governed by migrating and non-migrating tides. Since there's no wavenumber separation, it's impossible to distinguish migrating and non-migrating tidal signatures when calculating them at a fixed location. Hence, in this study, we are discussing the combination of both types of signatures extracted from the observatories, following Siddiqui et al. (2018a, b). The data corresponding to the period spanning March 5–6th, 1981 from both the observatories has been excluded due to the anomalous trend of the revised Dst index.

The signatures of the EEJ solar tides will be further compared with the derived current densities from the

Equatorial Electrojet model (EEJM-2.0), to see the coherence between the ground and satellite modelled datasets. The details of the EEJM-2.0 are described in Alken and Maus (2007). We obtained the current densities from EEJM-2.0 for daylight hours of all days at ETT longitude for the year 2002 after the calculation of real-time EUVAC (Extreme Ultra Violet flux model for Aeronomic Calculations) values (Richards et al. 1994) (http://omniweb.gsfc.nasa.gov/form/dx1.html).

The observed EEJ and Sq amplitudes at ETT and HYB after removing the revised Dst index for the years 1980–2002 are shown in Fig. 2.

In this study, we have followed two approaches: (I) Estimation of Sq and EEJ solar tidal signatures following Siddiqui et al. (2018a, b) and, (II) Power spectrum analysis following Gaspereni and Forbes (2014) to know the periodicities of $\sqrt{F10.7}$, Sq, EEJ and their correlation with solar rotation and solar cycle variability.

Estimation of the solar tidal variations from the Sq and EEJ strength

The S1 and S2 are the main dominant tidal signatures of the Sq and EEJ. In addition, the lunar tidal variation also plays a vital role on the Sq and EEJ with a significant effect on the lunar semi-diurnal (12.42 solar hours) component.

The S variations from the Sq and EEJ are estimated using Chapman's phase law (Malin and Chapman 1970) and written as:

$$S_n = s_n \sin\left(\frac{2\pi}{24}nt + \sigma_n\right) \tag{2}$$

where s_n and σ_n are the amplitude and phase of the n^{th} harmonic component.

The S variations are assessed for four Fourier coefficients ($n = 1, 2, 3, 4$) through a least square fitting approach using the following equation:

$$S = \sum_{n=1}^{4} s_n sin\left(\frac{2\pi}{24}nt + \sigma_n\right) \tag{3}$$

This study uses 5-day running window to carry out the least square fitting method. We have also derived the amplitude of the different tidal signatures and assigned them to their corresponding central days during the fitting of the tidal signatures within each running window (Siddiqui et al. 2018a, b).

Power spectrum analysis

The power spectra are applied to the Sq, EEJ, and $\sqrt{F10.7}$ for the entire year to determine the periodicities present

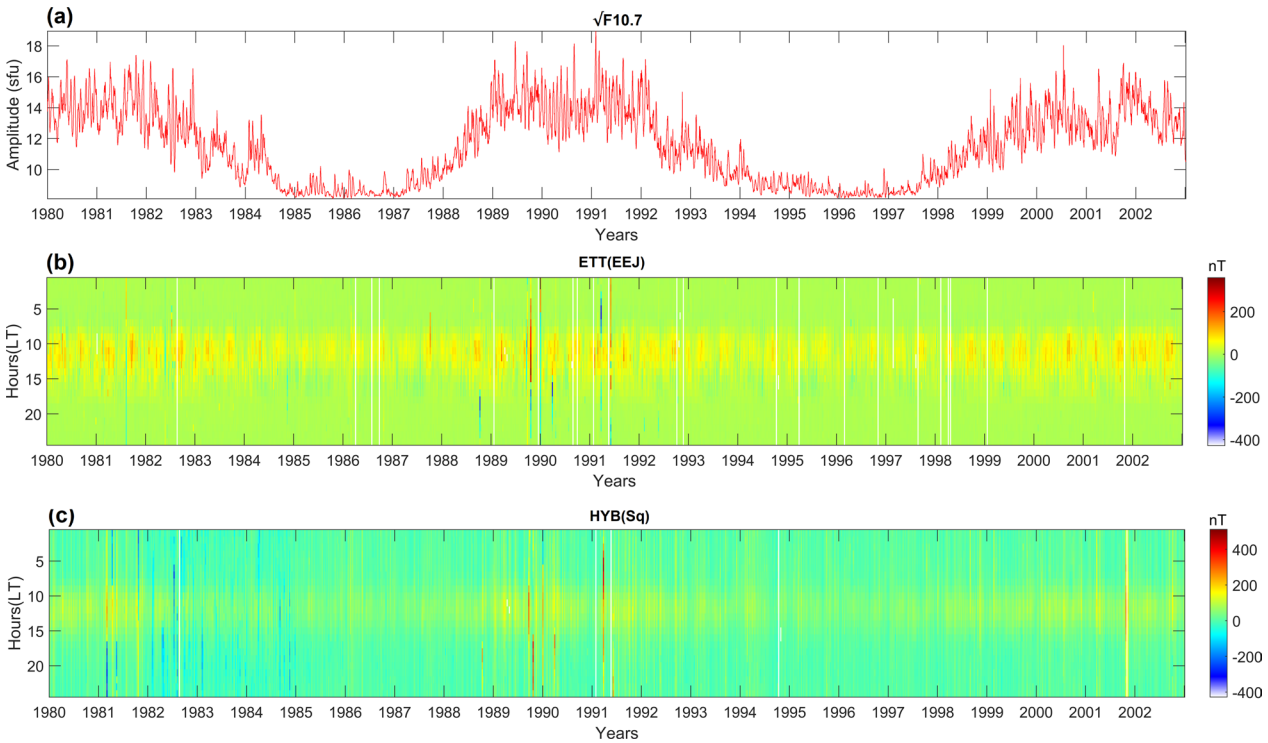

Fig. 2 The hourly mean data of **a** $\sqrt{F10.7}$, **b** EEJ strength at ETT after subtracting the revised Dst, **c** Sq strength of HYB after removing the revised Dst for the years 1980–2002. White colour vertical lines at both the observatories represents the loss of data (in hours as well as days)

in the data. The power spectra are estimated by the fast Fourier transform (FFT) squared magnitude. The sampling period of the ΔH measurements is taken once per hour which providing a Nyquist period of two hours.

Results and discussion

Characteristics of Sq and EEJ solar tidal signatures

a) With solar cycle phases

The obtained S1, S2, S3, and S4 tidal signatures of Sq and EEJ are shown in Figs. 3 and 4 for the period 1980–2002. The change in the tidal amplitudes follow a similar pattern corresponding to $\sqrt{F10.7}$ (11-year solar cycle variation) (Fig. 2a). The variation of $\sqrt{F10.7}$ correlates well with the Sq and EEJ where more ionization in the atmosphere corresponds to more intensity in Sq as well as in EEJ and vice versa. The changes in solar tidal amplitudes on the Sq and EEJ concerning different phases are evaluated by accounting minimum, ascending, maximum and descending phases of the solar cycles (21–23). We have calculated the mean of each phase to report the tidal amplitude variations associated with the solar cycle trends. The classification details of each phase for solar cycles 21–23 can be found in Text s2. The below paragraphs describe the response of solar tidal signatures on the Sq and EEJ amplitudes, respectively.

Figure 3 shows that S1, S2, S3 and S4 tidal amplitudes follow the trend of solar cycle pattern for the 23 years. The solar tidal signatures of the Sq show annual variations with larger amplitudes during summer maximum and the semi-annual variation during equinoctial minima (Fig. 3). Table 1 provides the details of the variability in the Sq solar tidal amplitudes during different SC phases. It is clear from the table that the S1 is maximum (30.6 nT) during 21st SC when compared to 22nd (26.7 nT) and 23rd SC (25.6 nT) during the maximum phase. Similarly, for S2 we have noticed that the amplitude is maximum in 21st SC (14.1 nT), and is found to be similar for 22nd (12.6 nT) and 23rd (12.8 nT) SCs during maximum phase. Whereas, for S3 and S4 the tidal amplitude is high in 21st SC (6.3 nT and 2.9 nT) and found to be nearly the same (~ 5.5 nT and ~ 2 nT) during the maximum period for the cycles 22–23. For descending phase, amplitude of S1 is maximum in 21nd SC (21.8 nT) and minimum in 22nd SC (19.2 nT). The tidal amplitudes of S2, S3 and S4 (10.7 nT, 5 nT and 2.7 nT) in 21st SC are higher than in 22nd SC tidal amplitudes (9.6 nT, 4.2 nT and 1.7 nT). Similarly, the amplitude of S1 is again maximum in 21st SC (16.7 nT) and minimum in 22nd SC (15.4 nT) during minimum phase. The tidal amplitudes of S2, S3 and S4 (8.5 nT, 3.9 nT and 1.8 nT) in 21st SC are larger in comparison to 22nd SC tidal amplitudes (7.6 nT, 3.4 nT and 1.4 nT).

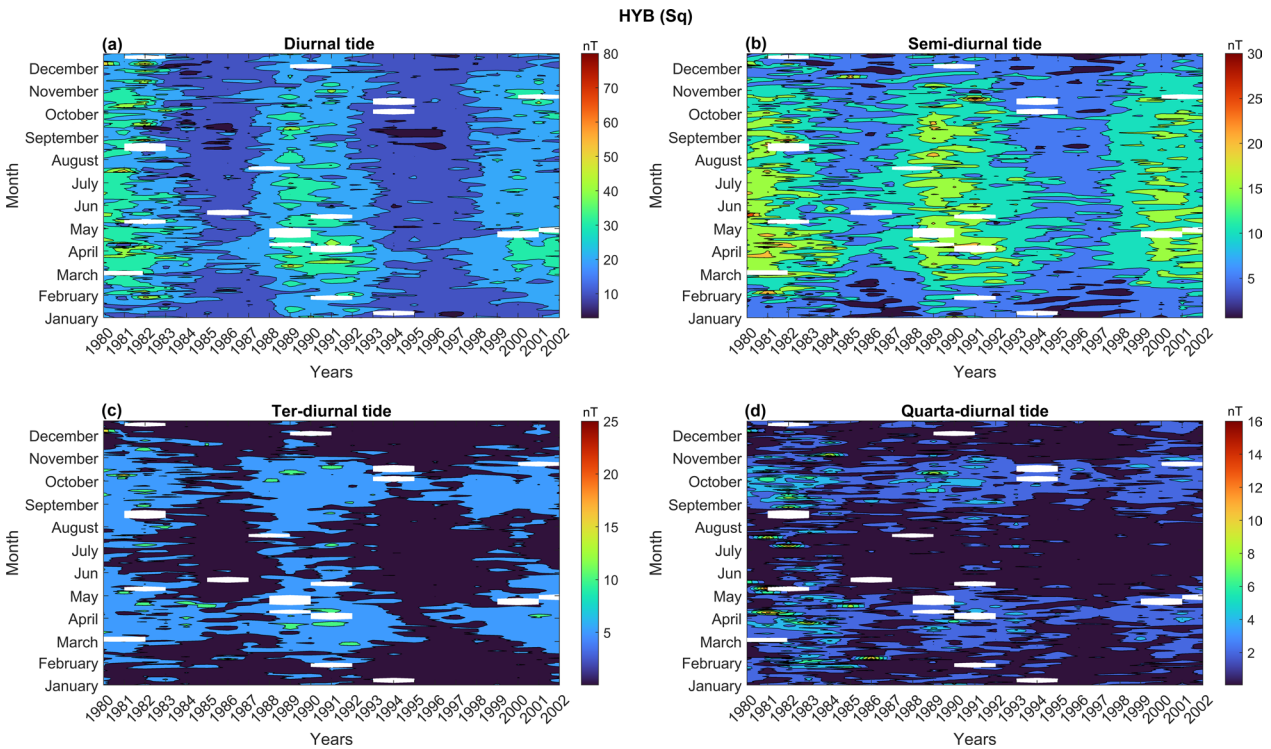

Fig. 3 The amplitude variations and characteristics of the different solar tides of the Sq (S1, S2, S3 and S4) for the period 1980–2002

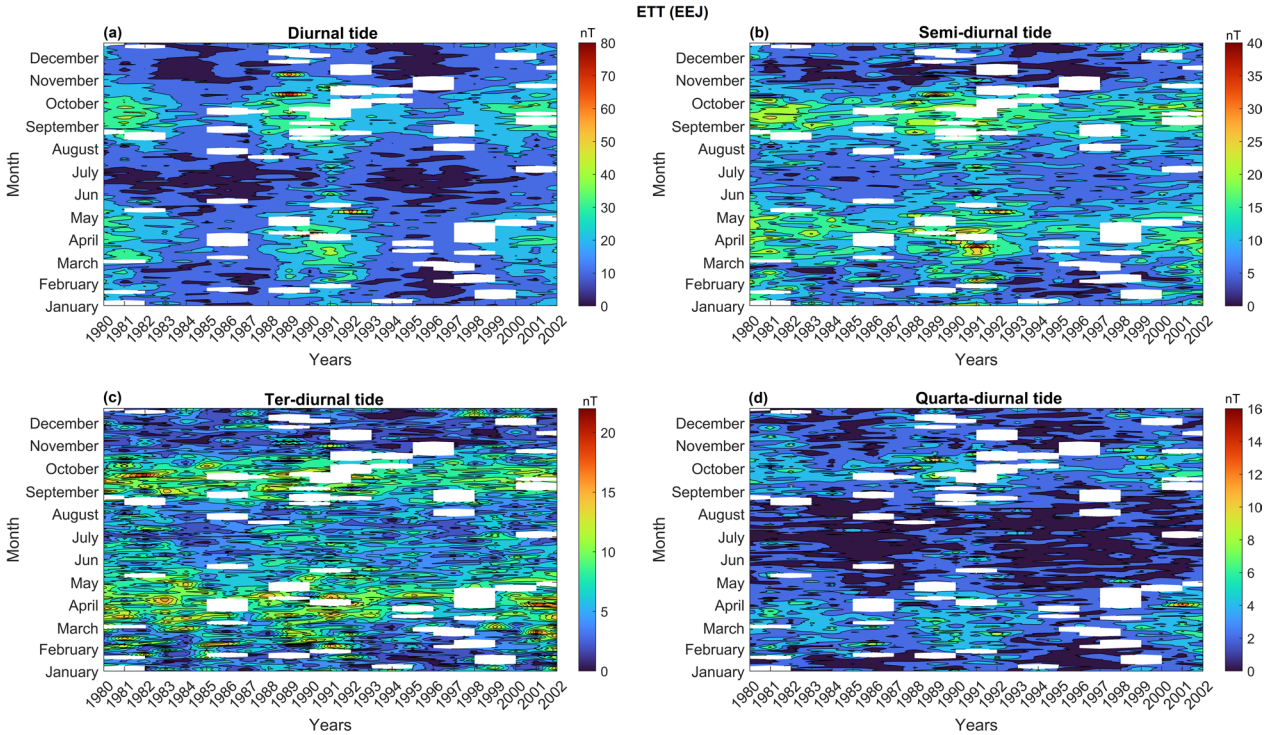

Fig. 4 The amplitude variations and characteristics of the different solar tides (S1, S2, S3 and S4) of the EEJ from 1980 to 2002

These tidal amplitudes follow the same pattern for the ascending phase of 21–22 SCs.

In summary, from our analysis and Table 1, it is evident that the overall Sq solar tidal amplitudes are found to be 55.6% (S1), 27.2% (S2), 12.2% (S3), and 5% (S4), respectively during SC: 21–23. Additionally, the observations of Sq solar tidal amplitudes are found to be strong during 21st SC when compared to SC-22 and 23 by ~ 13% and 16%, which is in contrast with Venkat Ratnam et al. [2014], who reported higher tidal amplitudes in the solar minimum at Gadanki using MST Radar/Radiosonde and ERA-interim data sets during SCs: 21–23.

Figure 4 shows the strong amplitudes of S1, S2, S3, and S4 with semi-annual variation during March/April and September/October. Table 2 provides the details of the variability in the EEJ solar tidal amplitudes (S1, S2, S3, and S4) during different SC phases. It is evident from the table that the S

1 is maximum (24.2 nT) during 22nd SC when compared to 21st and 23rd SC (22.1 nT) each. Similarly, for S2, we found the same trend in the amplitude with a maximum in the 22nd SC (13.5 nT), intermediate in the 21st (13.2 nT), and minimum in the 23rd SC (12.6 nT), respectively. Whereas for S3 and S4, the tidal amplitudes are found to be ~ 7 nT and ~ 3 nT, respectively, during the SC maximum period for the cycles 21–23. Further, the Sq and EEJ tidal signatures show a direct relationship with the decrease in the amplitude as the degree of harmonics (n) increases.

In summary, all tidal amplitudes of EEJ are found to be strong in SC-22 during its maximum period compared to SC: 21 and 23 by ~ 9%, indicating that SC-22 has a stronger response on the EEJ. This could be because of the higher solar flux level with varying ionospheric conductivity (Arora et al. 1984; Alken and Maus 2007). For the descending phase, the amplitude of S1 is maximum in 22nd SC (16.2 nT) and minimum in 21st SC (15.6 nT). In contrast, we found maximum amplitudes of S2, S3, and S4 in the minima and ascending phases of SC-21 when compared to SC-22, which is an important observation from this study and the reason for the lowered tidal signatures during SC-22 could be attributed to higher occurrence rate of strong CEJs in SC-22 at ETT (Chandrasekhar and Roy 2020). From our analysis and Table 2, the EEJ consists of S1, S2, S3, and S4 amplitudes by 46.3%, 29.2%, 17.0%, and 7.5%, respectively.

Based on all the above observations from Sq and EEJ, we deduce that the S1 tidal amplitude of Sq is always higher than the EEJ amplitude for all the SC phases by ~ 10%. Whereas, S2, S3, and S4 tidal amplitudes of Sq are lower than EEJ tidal amplitudes by ~ 2%, 5%, and 2.5%, respectively. From Tables 1 and 2, it is

Table 1 Changes in mean solar tidal amplitudes of the Sq during different solar cycle phases with standard error (±)

21st solar cycle					22nd solar cycle					23rd solar cycle				
Solar phase	**S1**	**S2**	**S3**	**S4**	**Solar phase**	**S1**	**S2**	**S3**	**S4**	**Solar phase**	**S1**	**S2**	**S3**	**S4**
Maximum (1980–1982)	30.4 ± 8.1	14.1 ± 4.4	**6.3** ± 2.7	**2.9** ± 2.1	Maximum (1990–1992)	26.7 ± 6.2	**12.6** ± 3.8	**5.8** ± 2.2	**2.1** ± 1.2	Maximum (2000–2002)	25.6 ± 5.5	12.8 ± 3.7	**5.4** ± 1.8	**2.0** ± 1.0
Descending (1982–1985)	21.8 ± 8.7	**10.7** ± 3.9	**5.0** ± 2.5	**2.7** ± 1.8	Descending (1992–1995)	19.2 ± 6.1	**9.6** ± 3.1	**4.2** ± 1.9	**1.7** ± 1.0	–	–	–	–	–
Minimum (1985–1987)	16.7 ± 3.8	**8.5** ± 2.7	**3.9** ± 1.8	**1.8** ± 1.2	Minimum (1995–1997)	15.4 ± 3.5	**7.6** ± 2.3	**3.4** ± 1.4	**1.4** ± 0.9	–	–	–	–	–
Ascending (1987–1990)	24.7 ± 7.0	12.1 ± 4.1	**5.3** ± 2.0	**2.0** ± 1.3	Ascending (1997–2000)	21.2 ± 5.9	**10.7** ± 3.7	**4.4** ± 1.7	**1.7** ± 0.9	–	–	–	–	–

Note: The values of the solar tidal amplitudes (S1, S2, S3, and S4) are reported in nT. The bold values will be compared with the EEJ tidal amplitudes in Table 2

Table 2 Changes in mean solar tidal amplitudes of the EEJ during different Solar cycle phases with standard error (±)

21st solar cycle					22nd solar cycle					23rd solar cycle				
Solar phase	**S1**	**S2**	**S3**	**S4**	**Solar phase**	**S1**	**S2**	**S3**	**S4**	**Solar phase**	**S1**	**S2**	**S3**	**S4**
Maximum (1980–1982)	22.1 ± 9.2	13.2 ± 5.6	**7.2** ± 3.4	**3.3** ± 1.6	Maximum (1990–1992)	24.2 ± 9.5	**13.5** ± 5.8	**7.2** ± 3.2	**3.6** ± 1.7	Maximum (2000–2002)	22.1 ± 7.2	12.6 ± 4.7	**7.1** ± 3.5	**3.4** ± 1.8
Descending (1982–1985)	15.6 ± 7.1	**10.9** ± 4.8	**6.8** ± 3.4	**2.9** ± 1.5	Descending (1992–1995)	16.2 ± 7.0	**10.2** ± 4.6	**6.1** ± 2.9	**2.7** ± 1.4	–	–	–	–	–
Minimum (1985–1987)	12.9 ± 4.8	**10.1** ± 3.9	**6.4** ± 2.8	**2.5** ± 1.4	Minimum (1995–1997)	12.4 ± 5.5	**9.1** ± 4.1	**5.5** ± 2.6	**2.1** ± 1.0	–	–	–	–	–
Ascending (1987–1990)	19.8 ± 10.2	12.1 ± 5.3	**6.9** ± 3.0	**3.2** ± 1.7	Ascending (1997–2000)	17.6 ± 6.8	**10.8** ± 4.1	**6.3** ± 2.8	**2.8** ± 1.5	–	–	–	–	–

Note: The values of the solar tidal amplitudes (S1, S2, S3, and S4) are reported in nT

evident that the tidal amplitudes of Sq are lower than EEJ for twenty-four cases out of thirty-six during different SC phases [marked as bold text] and vice versa for twelve cases. The semi-annual variation of the solar tidal amplitudes in EEJ is found to be more prominent during years of solar maximum activity, whereas for solar minimum years, the semi-annual peak is found to be greater in March/April than in September/October (Rastogi and Iyer 1976). The annual variation of Sq solar tidal amplitudes is more prominent during summer maximum (Wardinski and Mandea 2006; Celik et al. 2012) and found minima in semi-annual variation during equinoctial months (Lyatsky and Tan 2003). The derived Sq and EEJ solar tides show decreasing in amplitude during the minima phase of SC and vice versa. These results are consistent with the recent study of Soares et al. (2022), who found decrease in S1 and S2 amplitude trends from 2015 to 2018.

The computed Pearson correlation coefficients (P) between the mean of $\sqrt{F10.7}$ in each solar cycle phase and the obtained Sq tidal signatures (S1, S2, S3, and S4) are shown in Table 3. We have classified the 'P' coefficient in the following manner: (i) Strong positive $P \geq 0.9$, (ii) $0.7 \leq$ moderate $P < 0.9$, (iii) $0 \leq$ weak $P < 0.7$, and iv) negative $P < 0$.

The table shows a strong positive correlation during solar maximum, descending, minimum, and ascending phases between the mean of $\sqrt{F10.7}$ and S1 in SC-21. In the case of S2 and S3, P shows strong positive for all the phases except the minimum and maximum phase of SC-21 with moderate P. In S4, the P behaviour is found to be negative during maximum and minimum phases, strongly positive P during the solar descending phase, and moderate P during the solar ascending phase of SC-21. In SC-22, except in the minimum phase moderate and weak P is observed in S1–S2, negative P is observed in S3 and S4, and weak P is noticed in S4 during the maximum phase. The remaining other phases of SC-22 show strong positive P in S1–S4 solar tides. During the 23rd solar cycle, P is found to be moderate for all the tidal amplitudes except for the negative P noticed for S1 during the solar maximum phase.

The S2 of Sq solar tide follows a prominent 11-year cycle for the years 1980–2002 and is consistent with the results of Yamazaki and Kosch (2014). Moreover, the five-year average of S2 tidal amplitudes from the above study vary between 8.9 and 12.9 nT for eight stations, and closely corroborates with our derived tidal amplitudes at HYB, which are in the range of 7.6 and 14.1 nT.

Further, the decrease in correlation between $\sqrt{F10.7}$ and the tidal signatures (Table 3) shows a strong dependence on SSW during the 22nd SC minimum phase (i.e., 1995–1997), which could be due to the coupling of the stratosphere and the ionosphere and corroborates with the findings of Yamazaki (2013) and Bolaji et al. (2016) and the correlation between them found to be strong during the other phases of SCs.

The computed P between the mean of $\sqrt{F10.7}$ in each solar cycle phase and the obtained EEJ tidal amplitudes (S1–S4) are shown in Table 4. The table shows that strong positive P is observed during the solar maximum, descending, and ascending phases between the mean of $\sqrt{F10.7}$ and S1. In contrast, P is negative during the solar minimum phase of SC-21. In S2, P shows a strong positive during ascending phase, moderate P during the solar maximum and descending phases, and a negative during the solar minimum phase. In contrast, in S3, strong positive P is noticed during the solar maximum and ascending phases, and weak P during descending and solar minimum phases is noticed in SC-21. In S4, P is found to be strongly positive during descending and ascending phases, weak P during the solar minimum phase, and negative P during the solar maximum phase of SC-21.

In SC-22, a strong positive P is noticed during all SC phases of S1, whereas for S2, it is strongly positive during maximum, descending, and ascending phases and moderate during the solar minimum phase. The correlation is moderate during the solar maximum, descending, and ascending phases and weak during the solar minimum phase in S3. Again, strong positive P during descending and ascending phases and moderate P is observed during solar maximum and minimum phases in the S4 solar tidal component. During the 23rd solar cycle, P is found to be negative for all the tidal signatures during the maximum phase of SC.

We have only thirteen cases where EEJ and Sq behave similarly with $\sqrt{F10.7}$ (strong positive P) [marked as Bold text] and two cases where EEJ and Sq show negative P [marked as Italic text] out of thirty-six cases (Tables 3 and 4).

The instances of strong, moderate and weak positive, and negative of P are shown in Table 4. In this study, P reflects the nature of strong westward currents during daylight hours at ETT, which has resulted in weak tidal amplitudes during different phases of SC: 21–23. Chandrasekhar and Roy (2020) performed principal component analysis (PCA) on the historical ETT-EEJ and HYB-Sq datasets over 23 years (1980–2002) and reported normal (PC1) and abnormal fields (PC3) of Sq and EEJ during different phases of SC: 21–23. Their study also reported the occurrence of strong CEJs which are found to be more during SC minimum phase. Similarly, noticeable strong negative amplitudes are in records for the maxima, minima, descending, and ascending phases of SC: 21–23. Therefore, the strong positive P in this study

Table 3 Correlation between √(F10.7) and solar tidal amplitudes (S1, S2, S3, and S4) of the Sq during different solar cycle phases

21st solar cycle					22nd solar cycle					23rd solar cycle				
Solar phase	**S1**	**S2**	**S3**	**S4**	**Solar phase**	**S1**	**S2**	**S3**	**S4**	**Solar phase**	**S1**	**S2**	**S3**	**S4**
Maximum (1980–1982)	**0.98**	0.99	0.81	*− 0.74*	Maximum (1990–1992)	**0.96**	**0.92**	0.94	0.70	Maximum (2000–2002)	*− 0.25*	0.56	0.68	0.58
Descending (1982–1985)	**0.99**	0.99	0.95	**0.91**	Descending (1992–1995)	**0.98**	**0.98**	0.97	**0.95**	–	–	–	–	–
Minimum (1985–1987)	0.98	0.88	0.92	− 0.20	Minimum (1995–1997)	0.77	0.52	− 0.13	− 0.67	–	–	–	–	–
Ascending (1987–1990)	**0.98**	**0.98**	**0.99**	0.79	Ascending (1997–2000)	**0.99**	**0.99**	0.95	**0.99**	–	–	–	–	–

Note: (i) Strong positive $P \geq 0.9$, (ii) $0.7 \leq$ moderate $P < 0.9$, (iii) $0 \leq$ weak $P < 0.7$, and (iv) negative $P < 0$. Bold text shows the strong positive correlation observed between Tables 3 and 4, vice versa for negative correlation highlighted with Italic text

Table 4 Correlation between √(F10.7) and solar tidal amplitudes (S1, S2, S3, and S4) of the EEJ during different solar cycle phases

21st solar cycle					22nd solar cycle					23rd solar cycle				
Solar Phase	**S1**	**S2**	**S3**	**S4**	**Solar Phase**	**S1**	**S2**	**S3**	**S4**	**Solar Phase**	**S1**	**S2**	**S3**	**S4**
Maximum (1980–1982)	**0.97**	0.84	0.95	*− 0.07*	Maximum (1990–1992)	**0.93**	**0.96**	0.88	0.81	Maximum (2000–2002)	*− 0.99*	− 0.87	− 0.47	− 0.56
Descending (1982–1985)	**0.96**	0.75	0.25	**0.96**	Descending (1992–1995)	**0.99**	**0.93**	0.87	**0.99**	–	–	–	–	–
Minimum (1985–1987)	− 0.56	− 0.71	0.21	0.15	Minimum (1995–1997)	0.98	0.74	0.28	0.78	–	–	–	–	–
Ascending (1987–1990)	**0.98**	0.91	**0.99**	0.98	Ascending (1997–2000)	**0.98**	**0.96**	0.89	**0.90**	–	–	–	–	–

Note: (i) Strong positive $P \geq 0.9$, (ii) $0.7 \leq$ moderate $P < 0.9$, (iii) $0 \leq$ weak $P < 0.7$, and (iv) negative $P < 0$. Bold text shows the strong positive correlation observed between Tables 4 and 3, vice versa for negative correlation highlighted with Italic text

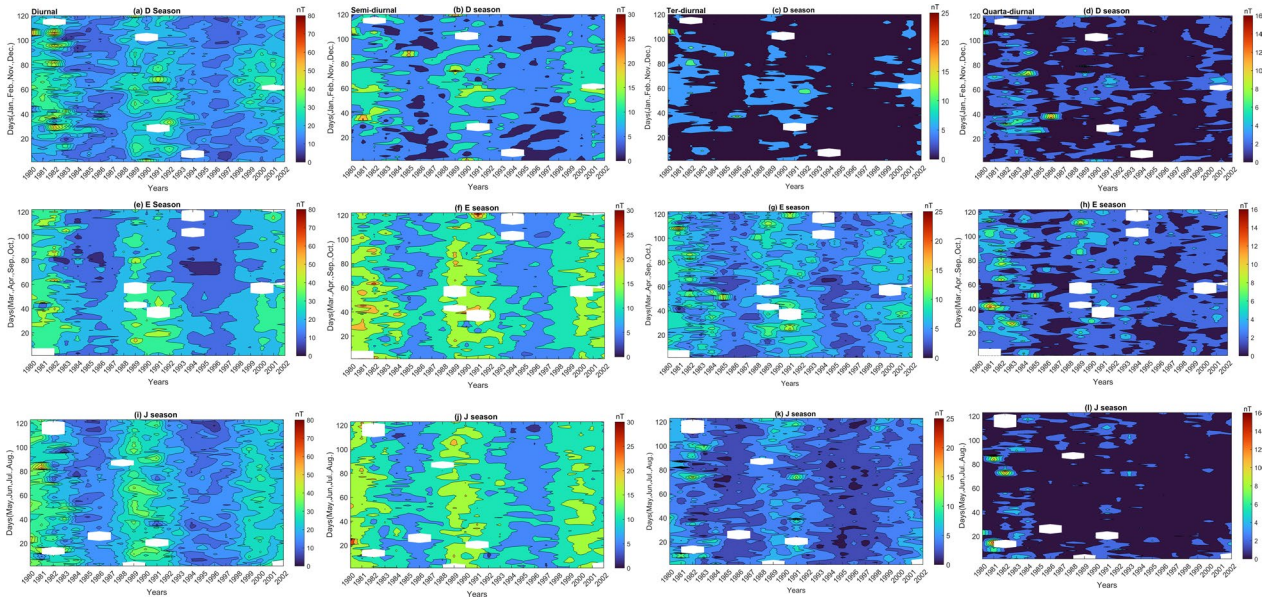

Fig. 5 Seasonal characteristics of the solar tides of the Sq during D, E, and J seasons for the period 1980–2002

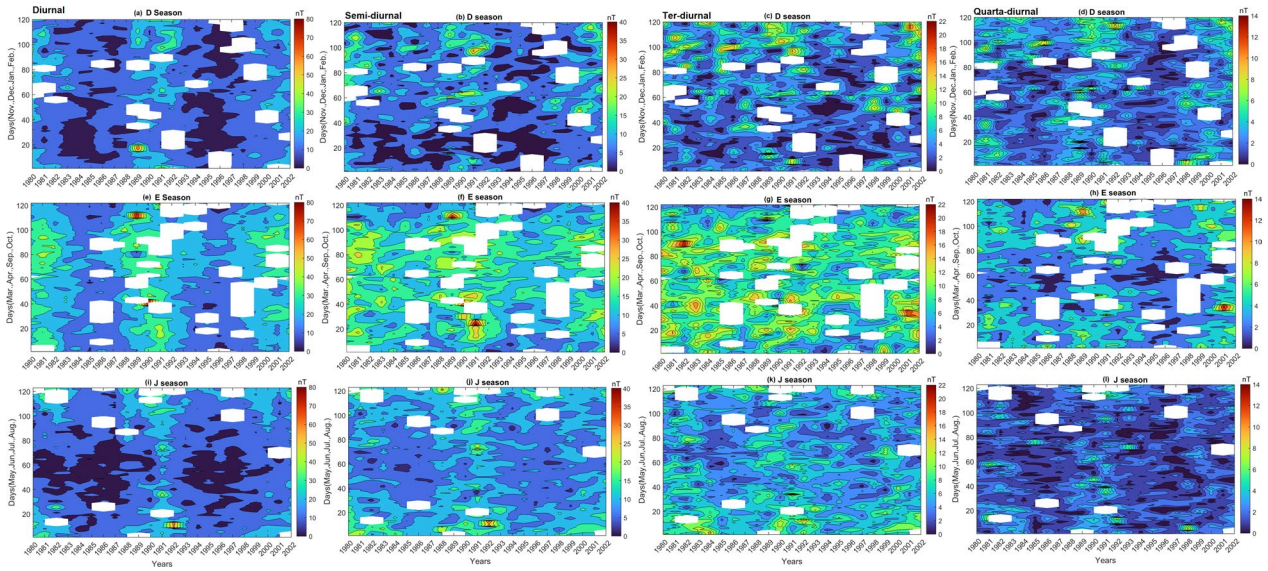

Fig. 6 Seasonal characteristics of the solar tides of the EEJ during D, E, and J seasons for the period 1980–2002

represents the close correspondence with the normal fields (PC1) and $\sqrt{F10.7}$. On the other hand, the moderate to negative P showcases the obstruction of the EEJ dominated by the strong CEJs during dissimilar solar cycle phases (Chandrasekhar and Roy 2020). The observed weak correlations in P due to CEJs at ETT during maxima and minima phases of SCs are in coherence with the records of SSW events. By examining Table 1 of Siddiqui et al. 2018a, b, Chandrasekhar and Roy (2020) have identified six split and seven displaced QBO (Quasi-biennial oscillation) vortex SSW events from February 29, 1980 to January 2, 2002. The observed CEJs at ETT during the winter solstice in 1985, 1987, 1988, 1989, 1999, and 2001 are attributed to the vortex split SSWs. Similarly, the CEJs observed in 1980, 1981, 1984, 1987, 1998, 2000, and 2002 are due to the vortex displaced SSWs. The decreased correlation between $\sqrt{F10.7}$ and the tidal signatures of EEJ/Sq (Tables 3 and 4) may be explained

by SSWs, and this finding is consistent with the results of Yamazaki (2013). Apart from this, the CEJs observed at ETT during the period (1982–83, 1986, 1990–97) could be due to the role of non-migrating diurnal tides of eastward and westward propagation as well as meteorological phenomena related to upper mesospheric wind, density variations, and temperature (Chandrasekhar et al. 2014, 2017). From 1997 to 2002, it is observed that the occurrence of morning (M) and afternoon (A) CEJs are more at the TTB site during the ascending phase of the 22nd SC, as noted by Soraes et al. (2020). On the other hand, during the same period, the events are less frequently observed at ETT. This suggests that the CEJs are longitudinally dependent (Chandrasekhar et al. 2017). Additionally, Chandrasekhar and Roy (2020) reported a fair number of evening (E) CEJs during the above period, whereas Soraes et al. (2020) did not report any such events.

This study illustrates that CEJs are dependent on solar cycle variations, particularly on the solar radio flux. The occurrence rate of CEJs increases with a decrease in F10.7 intensities, as discussed (Gurubaran et al. 2016; Chandrasekhar and Roy 2020). Cherkos (2023) observed that the midday EEJ has grown stronger as F10.7, and sunspot numbers have increased during the tilted period. Conversely, during low solar activity, moderate and weak fluctuations in the EEJ current strength are detected in various longitudinal sectors, leading to the appearance of CEJs, as also observed by Soares et al. (2018). Further, the observed inverse relationships between solar activity and tides are consistent with the findings of Sun et al. (2022).

b) With seasons

The seasonal characteristics of the Sq and EEJ solar tides are evaluated by grouping the months into three Lloyd seasons (D season: November-February; E season: March, April, September, and October; J-season: May–August). Figures 5 and 6 show the seasonal characteristics of the different Sq and EEJ solar tides during the D, E, and J seasons from 1980 to 2002.

The S1 amplitude of the Sq follows the solar cycle trend in all seasons (Fig. 5a, e, and i). It reflects high to moderate amplitudes in the last few days in January, November, and early days of February and December during solar maximum of SC-21. In contrast, moderate to weak amplitudes are noticed for the SC-22 and 23, respectively (Fig. 5a). In E-season, the high amplitudes are only seen in the early days of March, whereas moderate to low amplitudes are noticed in the remaining months for the SC 21–23 (Fig. 5e). Meanwhile, the J-seasonal S1 amplitudes are moderate in all SCs, and an enhancement signature can be seen mainly in SC-21 when compared to SC-22 and 23.

The S2 tidal amplitude of the Sq reflects the nature of solar cycle variations, displaying low to high amplitudes during February, November, and a few days in December during SC: 21–23, whereas the amplitudes are minimal during January month of SC: 21–22 in the D season (Fig. 5b). During the E season, S2 shows moderate to high amplitudes during solar maxima for SC: 21–23 (Fig. 5f). Meanwhile, in SC-21, the declining phase and solar minimum period recorded moderate tidal amplitudes. The tidal amplitude variations decrease prominently in SC: 22–23 compared to SC-21 (Fig. 5f). The variation of S2 tidal amplitude during the J season (Fig. 5j) follows the same trend as for the E season.

The S3 tidal amplitude of the Sq follows the trend of 11-year solar maxima for all three SCs (Fig. 5c, g, k). S3 tidal amplitude reflects moderate to low tidal amplitude for SC: 21–23 in D season (Fig. 5c). During the E season, the S3 shows moderate and low amplitude during solar maximum and minimum periods for all the SC's periods (Fig. 5g). The S3 tidal amplitude confirms moderate amplitude during the May and July months of SC: 21 and 22, whereas low tidal amplitude in SC-23 of the J season (Fig. 5k).

The S4 tidal amplitude of the Sq follows 11-year SC signature with moderate to high amplitude during the peak phase of SC-21 and low to moderate tidal amplitude during solar maximum of SC: 22–23 (Fig. 5d). Whereas in the E season, the S4 tidal amplitude follows the SC trend, reflecting high amplitudes during the September month for SC-21 and moderate to low tidal amplitude during the maxima of SC: 22–23 (Fig. 5h). In the J season, the S4 shows prolonged high amplitude for SC-21 in May and July, whereas the amplitudes are

Table 5 Correlation between $\sqrt{(}$F10.7)and seasonal solar, tidal amplitudes of the Sq and EEJ

Sq					EEJ				
Season	**S1**	**S2**	**S3**	**S4**	**Season**	**S1**	**S2**	**S3**	**S4**
D	0.9	0.92	0.89	0.43	D	0.91	0.83	0.66	0.87
E	0.96	0.95	0.91	0.64	E	0.97	0.85	0.65	0.89
J	0.93	0.93	0.92	0.39	J	0.78	0.76	0.73	0.75

Note: (i) Strong positive $P \geq 0.9$, (ii) $0.7 \leq$ moderate $P < 0.9$, (iii) $0 \leq$ weak $P < 0.7$, and (iv) negative $P < 0$

moderate and lowest during the SC: 22 and 23, respectively (Fig. 5l).

Overall, S1 tidal amplitudes of Sq reflect high intensity in the J season, followed by the E and D seasons, whereas the S2 and S3 solar tidal amplitudes show stronger intensity in the E season, followed by J and D seasons. The S4 tidal amplitude shows high intensity in the E season, followed by the D and J seasons.

The seasonal characteristics of the EEJ solar tides are discussed here. The S1 amplitudes of the EEJ follow the trend of the solar cycle in all seasons (Figs. 6a, e, and i), reflecting the moderate amplitudes of S1 during solar maximum in January and February, a few days in November (Fig. 6a). In E-season, the S1 shows moderate amplitude in the months of March, April, and September during solar maximum phase for all SCs, and strong amplitudes for a few days in October for the SC-22, while for SC-23 moderate amplitudes are observed for the first few days in April and September (Fig. 6e). Meanwhile, the J-seasonal S1 amplitudes are moderate, especially in May and August in all SCs solar maximum phases, and a prolonged signature of enhancement is seen, particularly in SC-22, when compared to SC-21 and 23. The S1 tidal amplitudes are weaker during the minima phase of SC: 21–23 (Fig. 6i).

The S2 EEJ tidal amplitude reflects the nature of solar cycle variations, displaying moderate to high amplitudes during January, February, and a few days in December. In contrast, the amplitudes are low during November (Fig. 6b). Further, we have also observed moderate amplitude during the solar minimum period for January and February for SC-21, whereas the same is not evident for SC-22. During the E season, S2 shows moderate to high amplitudes during solar maxima for SC: 21–22, and noticeable amplitudes are seen during the declining phase of SC-21. Meanwhile, SC-22, during the declining phase and solar minimum period, recorded weak amplitudes compared to SC-21 during April. The amplitude variation is substantial during March and October for SC-22 compared to SC-21 and 23 (Fig. 6f). The variation of S2 tidal amplitude is observed to be at its maximum during May in the J season (Fig. 6j) and follows the SC maxima 22. However, the exact nature is not reflected in SC: 21 and 23.

The S3 EEJ tidal amplitude shows high amplitudes in the D-season for January–February and weak amplitudes during the November–December months. It follows the trend of 11-year solar maxima for all the three SCs (Fig. 6c). S3 shows moderate to high tidal amplitudes during SC-21 minima, and the exact nature is not observed in SC-22. E season also reflects the 11-year SC nature with moderate to high amplitudes in all the phases, an interesting feature observed in this study (Fig. 6g). During the J season, the S3 shows less intensity variations (Fig. 6k).

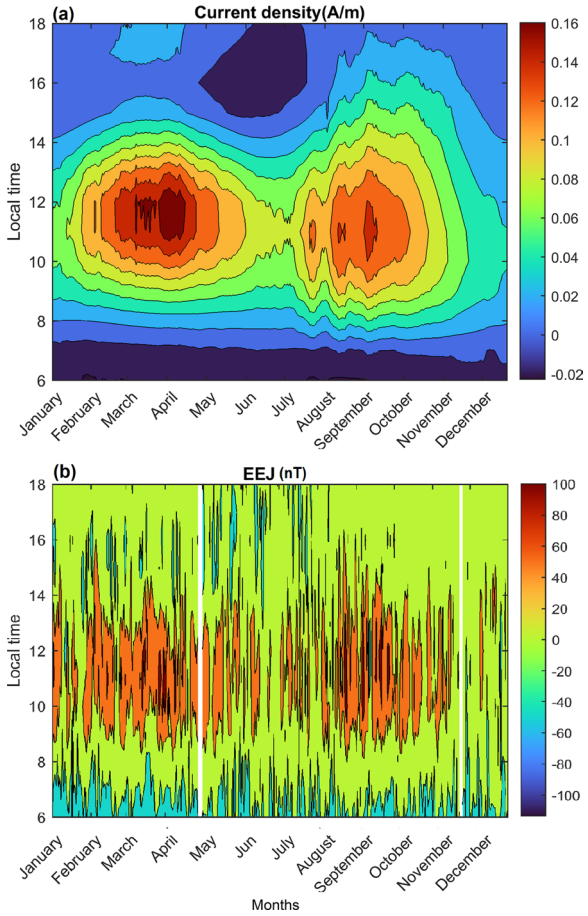

Fig. 7 Derived hourly (LT: 6:00–18:00) daily **a** current densities of the EEJ from EEJM-2.0 model, **b** ground EEJ strength for the solar maximum year 2002

The S4 EEJ tidal amplitude also shows an 11-year SC signature with moderate to high amplitude during the peak phase of SC: 21–23 and moderate to low amplitudes during descending and a solar minimum of SC-21 (Fig. 6d). Whereas in the E season, the S4 variations follow the SC trend, reflecting moderate to high amplitudes during the months of March and September for SC: 21–23, and recorded high amplitudes during the month of October in SC-22 as well as in March of SC-23 (Fig. 6h). In the J season, the S4 shows prolonged moderate to high amplitude for SC-22, for a few months in SC-21 and no significant amplitudes are observed in SC-23 (Fig. 6l).

Overall, S1 and S3 EEJ tidal amplitudes show high intensity in the E season, followed by the D and J seasons. In contrast, the S2 and S4 tidal amplitude reflects high intensity in the E season, followed by the J and D seasons.

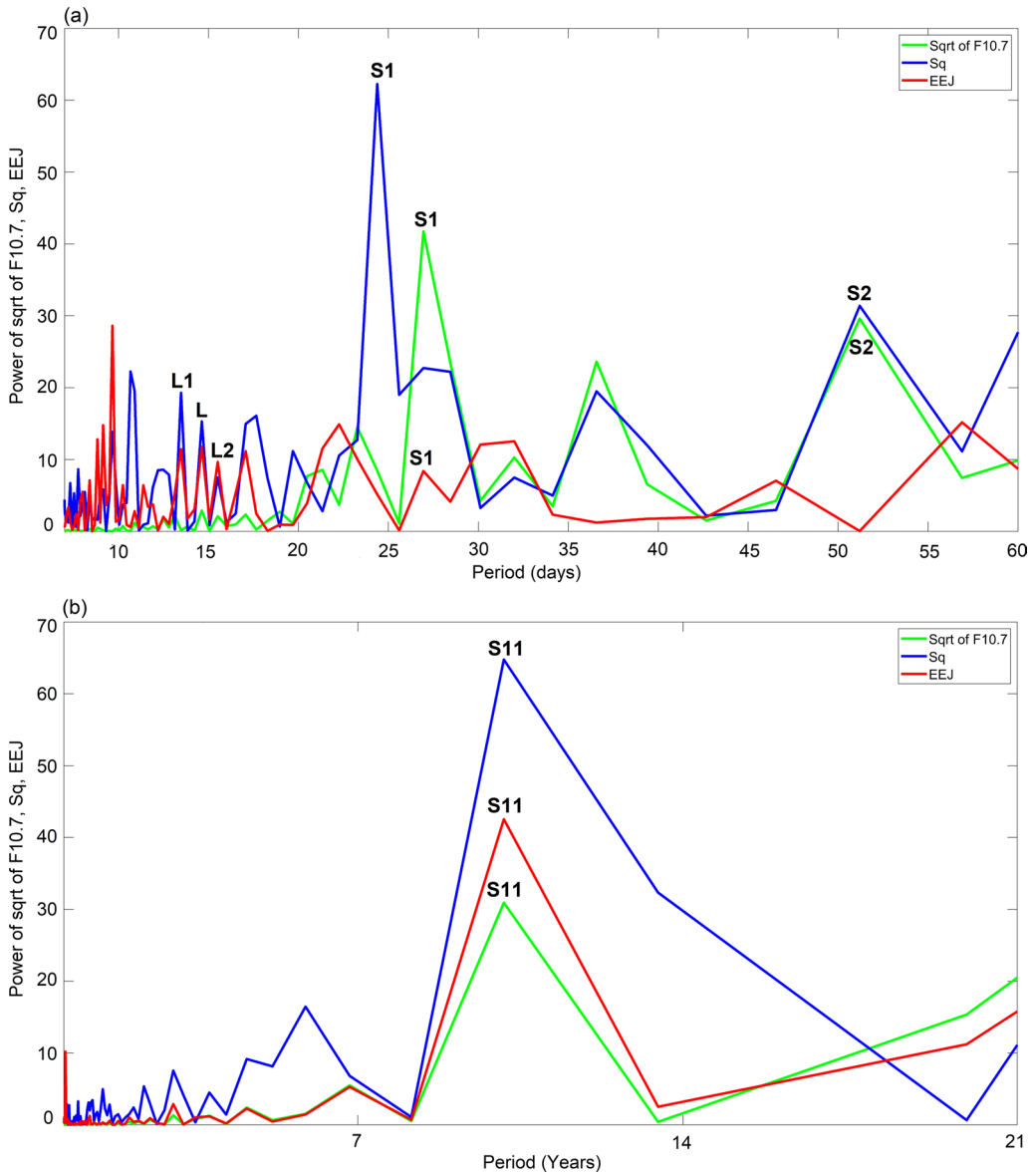

Fig. 8 Power spectral density of $\sqrt{F10.7}$, Sq, and EEJ as a function of **a** days, **b** years for 1980–2002

According to Takeda (2002), the tidal amplitudes of the geomagnetic field variation depend on solar activity and vary with the seasons. However, if the month is kept constant, the local ionospheric conductivity can largely explain the dependence on solar activity. This means that the local conductivity is the leading cause of the monthly dependence on solar activity. The tidal amplitude varies seasonally, with small values in winter and significant values in summer for the same conductivity values. This may be due to differences in neutral winds or magnetic effects from field-aligned currents between hemispheres caused by ionospheric dynamo asymmetry. Overall, the seasonal characteristics of solar tidal signatures S1–S4 on EEJ and Sq show the largest harmonic in equinoxes and the smallest in winter and summer solstices, which reinforces the earlier observations by Celik et al. (2012) and Sun et al. (2022).

Relationship between seasonal characteristics of Sq and EEJ solar tidal amplitudes with $\sqrt{F10.7}$

We have analyzed the relationship between S1, S2, S3, and S4 of Sq and EEJ tidal amplitudes with $\sqrt{F10.7}$ by calculating P on annual means to know the seasonal characteristics of these tides during D, E, and J seasons

(Table 5). From the table, for Sq solar tidal signatures, we have noticed strong positive P (S1 and S2), moderate P (S3), and weak P (S4) for the D season with $\sqrt{F10.7}$, whereas for E and J seasons, strong positive P (S1, S2, and S3) and weak P (S4) are observed. Similarly, for the EEJ tidal amplitudes, the relation is found to be strong positive P (S1), moderate P (S2, S4), and weak P (S3) during the D season with$\sqrt{F10.7}$. The relation is found to be strong positive P (S1), moderate P (S2, S4), and weak P (S3) in the E season for the EEJ solar tides with$\sqrt{F10.7}$. In J season, the correlation is moderate for all the tidal amplitudes with$\sqrt{F10.7}$. It is evident that during the E season, the solar tidal amplitudes of Sq and EEJ reflect strong correlation with $\sqrt{F10.7}$ compared to the D and J seasons. Further, our observations show strong coherence between $\sqrt{F10.7}$ and EEJ-S1 tide during E season, which is in agreement with Guharay et al. (2019) and in contrast with other tidal signatures (S2–S4). Additionally, we have also derived annual mean solar tidal amplitudes of Sq and EEJ as shown in Figure s2 and s3 (Additional file 1). From the Additional file 1: Figures S2 and S3, it is evident that the enhanced solar tidal amplitudes of Sq-S4 are not closely related to SC (Rastogi and Iyer 1976). Whereas, the remaining tidal signatures (S1–S3) and EEJ (S1–S4) have a strong correspondence with $\sqrt{F10.7}$.

Comparison of EEJ signatures with the EEJM-2.0

Figure 7 shows an example plot of the EEJ current density derived from the EEJM-2.0 model and hourly daily values (LT: 6:00–18:00) of observed EEJ ground data for the solar maximum year 2002. We have chosen this year for the comparison due to the availability of EEJM-2.0 data from 2002 onwards, and ETT data are available till the end of 2002. The high EEJ strength of current densities (~0.11–0.16 A/m) is observed during the months of March, April, September, and October (E-season) for the year 2002 (Fig. 7a), which significantly matches with the high EEJ strengths (~70–100 nT) at ETT (Fig. 7b). The moderate current densities (~0.08–0.13 A/m) are reflected in the month of May, June, July, and August (J-season), matches with the EEJ strength (~50–80 nT). The low current densities (~0.09 A/m) are observed in the months of January, February, November, and December (D-season) and corroborate with the EEJ ground data (~40–70 nT) in these months.

The overall EEJ signatures are in coherence with the EEJM-2.0 for the months discussed above with some deviations since the model may not be able to represent the inherent atmospheric parameters for daily variability in the solar tides. On closer observation, we have found that EEJ strength is high in the E-season followed by moderate, and weak in the J and D-seasons, respectively (Fig. 7b). These observations are in good coherence with the modelled output of the current density model (Fig. 7a). Contour variations in Fig. 7a are much smoother than ground data (Fig. 7b). To represent the smooth characteristics of ground-derived EEJ strength (comprised of solar tides) with EEJM-2.0, we have calculated the monthly hourly mean of the current densities and EEJ data simultaneously from 6:00 to 18:00 LT (Additional file 1: Figure S4). The results show that the overall EEJ current density distribution derived from the EEJM-2.0 strongly coincides with the observed signal derived from the ground magnetic data.

Power spectral density estimates: Sq and EEJ strength

To understand the relationship between $\sqrt{F10.7}$, Sq and EEJ strength, we have computed the power spectra by considering all the days from 1980 to 2002 (Fig. 8). Figure 8a shows the response of $\sqrt{F10.7}$, Sq and EEJ reflecting the intense 27 days solar rotation period as the dominant peak (S1 at 26.9 days) accounts for almost half of the entire spectrum and correlates well with the EEJ peak (S1 at 26.9 days) (Hamid et al. 2013). In contrast, the dominant peak at Sq is observed around 24.3 days (Fig. 8a), which coincides with $\sqrt{F10.7}$ and TEC as reported (Chakrabarty et al. 2012). The second dominant peak of $\sqrt{F10.7}$ is also observed (S2 at 51.2 days and 36.5 days), which correlates well with Sq but not with EEJ. This poor correlation of EEJ may be associated with the product of conductivity and the electric field parameter's current density, which are influenced by the solar tides (Luhr and Manoj 2013) and also by other factors like the lower atmosphere coupling as well as the role of local ionospheric conditions on the EEJ strength (Hamid et al. 2013). A certain dominant peak at a period of 32 days appears in these spectrums, which needs further validation with some physical parameters.

Figure 8a also shows the contribution of one dominant lunar tidal peak (L at 14.6 days) with side peaks (L1 at 13.5 days and L2 at 15.5 days) in EEJ (Gasperini and Forbes 2014) and Sq. We have also observed many low periodicity peaks (i.e., close to 2.5, 5.9, and 9 days) in Sq and EEJ due to the variations driven by the planetary wave oscillation as suggested (Parish et al. 1994; Hamid et al. 2013) and these signatures are not prominent in $\sqrt{F10.7}$.

Solar cycle variability is depicted in Fig. 8b by taking the power spectra of 27-days mean of Sq, EEJ, and $\sqrt{F10.7}$. It is evident from Fig. 8b that the 11-year solar dominant peak is reflected at 10.6 years (S11). This result shows that the E region conductivity variations due to solar radiation play an essential part in characterizing the EEJ variability.

Conclusions

This study investigates the response of solar tidal signatures S1–S4 (combination of migrating and non-migrating) and their seasonal characteristics in the Indian sector over the SCs: 21–23 during different phases. The following are the important outcomes of this study:

I. SC-21 has stronger response on Sq tidal amplitudes than SC-22 and SC-23 by ~ 13% and 16%.
II. SC-22 shows more variation in tidal amplitudes on EEJ by ~ 9%, when compared to the other solar cycles, which has not been addressed previously.
III. During SC: 21–23, the amplitude of the S1-Sq tide is consistently higher than EEJ tide by ~ 10%. For the same period, the S2-S4 tidal signatures of Sq are weaker than EEJ by ~ 2%, 5%, and 2.5%, respectively.
IV. The enhanced Sq solar tidal amplitude of S4 is not closely related to SC, whereas the remaining tidal signatures (S1–S3 of Sq) and (S1–S4 of EEJ) have a strong correspondence with $\sqrt{F10.7}$.
V. The annual variation of Sq solar tidal signatures is more prominent during summer maximum and the semi-annual variation during equinoctial minima.
VI. The semi-annual variation of the EEJ solar tidal signatures is more prominent during years of maximum solar activity. In contrast, for solar minimum years, the semi-annual peak is greater in March/April than in September/October.
VII. The moderate to negative correlations between $\sqrt{F10.7}$ and Sq/EEJ tidal amplitudes reflect the occurrence of CEJs during different phases of SCs: 21–23.
VIII. Power spectrum characteristics show 26.9 (~ 27) days peak corresponding to solar rotation variability, 14.6 days lunar tidal peak, and 10.6 years solar cycle period's signature in the Sq and EEJ, which well correlates with $\sqrt{F10.7}$.
IX. Low periodicity spectral peaks in Sq and EEJ followed by weak correlation with $\sqrt{F10.7}$ indicate the influences of the lower atmospheric forcing at these observatories.

The observed discrepancy between the Sq and EEJ solar tidal signatures at a lateral separation of 900 km from this study needs further assessment by comparing the observations with other longitudes. Keeping in view of the revised Dst index data availability, we would like to propose a global study at different longitudes of low-latitude and equatorial observatories as a future work, which provides a comprehensive picture of the actual physical processes responsible for the observed features bearing spatial variability between the observatories.

Supplementary Information

The online version contains supplementary material available at https://doi.org/10.1186/s40623-024-01996-8.

Additional file 1: Figure S1. Hourly mean variation data of all days after removing the midnight means for at each observatory for the years 1980–2002 (**a**) ETT and (**b**) HYB. Note: White colour vertical lines at both observatories represents the loss of data (in hours as well as days). **Figure S2.** Derived annual mean solar tidal amplitudes of 1) S1, 2) S2, 3) S3, and 4) S4 of Sq. **Figure S3.** Derived annual mean solar tidal amplitudes of 1) S1, 2) S2, 3) S3, and 4) S4 of EEJ. **Figure S4.** Derived monthly hourly mean (LT: 6:00 to 18:00) **a** current densities of the EEJ from EEJM-2.0 model, **b** ground EEJ strength for the solar maxima year 2002.

Acknowledgements

We appreciate the comments of the two anonymous reviewers that significantly improved this manuscript. We thank the Director, NGRI, for encouraging us to submit this work; reference no. NGRI/Lib/2023/Pub-14. The authors wish to thank Dr. Kusumita Arora for her constant encouragement and permission to research the historical data set. Additionally, the authors are thankful to the colleagues of HYB and ETT Observatories for their valuable contribution toward data acquisition and digitization of photographic charts.

Author contributions

Divyanshu Dwivedi: Conceptualization, Methodology, Coding, Validation, Formal analysis, Investigation, Writing-original draft, Review and editing, Visualization. N. Phani Chandrasekhar: Conceptualization, Validation, Investigation, Writing-original draft, Review and editing, Visualization.

Funding

No funding was provided for this work.

Availability of data and materials

The raw data of hourly mean values of the horizontal field intensity of the geomagnetic field at ETT and HYB are available in the repository. The F10.7 data used in this study is available at https://omniweb.gsfc.nasa.gov/form/dx1.html. The revised Dst index has been taken from the site http://geomag.usgs.gov/products/downloads.php.Raw data of HYB and ETT Observatories are available https://www.ngri.res.in/files/dd/HYB_RAW_DATA_H_COMPONENT.zip.

Declarations

Competing interests

The authors declare that they have no competing financial interests or personal relationships that could have appeared to influence the work reported in this paper.

Author details

[1]Geomagnetism Group, CSIR-National Geophysical Research Institute, Hyderabad, India.

Received: 22 June 2023 Accepted: 26 March 2024
Published online: 28 April 2024

References

Alken P, Maus S (2007) Spatio-temporal characterization of the equatorial electrojet from CHAMP, Orsted and SAC-C satellite measurements. J Geophys Res 112:A09304. https://doi.org/10.1029/2007JA012524

Arora BR, Rao DRK, Sastri NS (1984) Solar and lunar daily variations at alibag. Pure Appl Geophys 122:89–109. https://doi.org/10.1007/BF00879651

Bolaji OS et al (2016) Solar quiet current response in the African sector due to a sudden stratospheric warming event. J Geophys Res Space Phys 121:8055–8065. https://doi.org/10.1002/2016JA022857
Çelik C et al (2012) Solar and lunar geomagnetic variations in the northwestern part of Turkey. Geophys J Int 189(1):391–399. https://doi.org/10.1111/j.1365-246X.2012.05382.x
Chandrasekhar NP, Roy A (2020) Imprints of sunspot cycles on normal and abnormal geomagnetic fields: Cases study from equatorial and low-latitude sites of India. J Geophys Res Space Phys 125:e2020JA028464. https://doi.org/10.1029/2020JA028464
Chandrasekhar NP, Arora K, Nagarajan N (2014) Evidence of short spatial variability of the equatorial electrojet at close longitudinal separation. Earth Planets Space 66(1):1–15. https://doi.org/10.1186/1880-5981-66-110
Chandrasekhar NP, Archana RK, Nagarajan N, Arora K (2017) Variability of equatorial counter electrojet signatures in the Indian region. J Geophys Res Space Physics 122:2185–2201. https://doi.org/10.1002/2016JA022904
Chapman S (1951) The equatorial electrojet as detected from the abnormal electric current distribution above Huancayo and elsewhere. Archiv Für Meteorologie Geophysik Und Bioklimatologie A4:368–392. https://doi.org/10.1007/BF02246814
Charkrabarty D, Bagiya MS, Thampi SV, Iyer KN (2012) Solar EUV flux (0.1–50 nm), F10.7 cm 408 flux, sunspot number and total electron content in the crest region of the ionization anomaly during the deep minimum between solar cycle 23 and 24. Indian Radio Space Phys 41:110–120
Cherkos AM (2023) Solar flux effects on the variations of equatorial electrojet (EEJ) and counter-electrojet (CEJ) current across the different longitudinal sectors during low and high solar activity. J Astronomy Space Sci 40(2):45–57. https://doi.org/10.5140/JASS.2023.40.2.45
Forbes JM et al (2003) Nonmigrating diurnal tides in the thermosphere. J Geophys Res Space Phys 108(A1):1033. https://doi.org/10.1029/2002JA009262
Garcés M, Drob DP, Picone JM (2002) A theoretical study of the effect of geomagnetic fluctuations and solar tides on the propagation of infrasonic waves in the upper atmosphere. Geophys J Int 148(1):77–87. https://doi.org/10.1046/j.0956-540x.2001.01563.x
Gasperini F, Forbes JM (2014) Lunar-solar interactions in the equatorial electrojet. Geophys Res Lett 41:3026–3031. https://doi.org/10.1002/2014GL059294
Gouin P, Mayaud PN (1967) Apropos de 1′ existens possible d'un counter electrojet aux latitudes equatorials. Ann Geophys 23:41–50
Guharay A, Batista PP, Andrioli VF (2019) Investigation of solar cycle dependence of the tides in the low latitude MLT using meteor radar observations. J Atmos Solar Terr Phys 193:105083. https://doi.org/10.1016/j.jastp.2019.105083
Gurubaran S, Sathishkumar S, Veenadhari B (2016) On the role of atmospheric tides in the quiet-time variabilities of equatorial electrojet. J Indian Geophys Union 2:87–98
Hagan ME, Forbes JM (2003) Migrating and nonmigrating semi-diurnal tides in the upper atmosphere excited by tropospheric latent heat release. J Geophys Res 108:1062. https://doi.org/10.1029/2002JA009466
Hagan ME, Roble RG, Hackney J (2001) Migrating thermospheric tides. J Geophys Res Space Physics 106(A7):12739–12752
Hamid NSA, Liu H, Uozumi T, Yumoto K (2013) Equatorial electrojet dependence on solar activity in the Southeast Asia sector. Antarctic Record 57(3):329–337
Lindzen RS, Chapman S (1969) Atmospheric tides. Space Sci Rev 10(1):3–188
Love JJ, Gannon JL (2009) Revised Dst and the epicycles of magnetic disturbance: 1958–2007. Ann Geophys 27(3101–3131):2009. https://doi.org/10.5194/angeo-27-3101-2009
Lühr H, Manoj C (2013) The complete spectrum of the equatorial electrojet related to solar tides: CHAMP observations. Ann Geophys 31(1315–1331):2013. https://doi.org/10.5194/angeo-31-1315-2013
Lyatsky W, Tan A (2003) Latitudinal effect in semiannual variation of geomagnetic activity. J Geophys Res 108(A5):1204. https://doi.org/10.1029/2002JA009467
Malin SRC, Chapman S (1970) The determination of lunar daily geophysical variations by the Chapman-Miller Method. Geophys J Roy Astron Soc 19:15–35. https://doi.org/10.1111/j.1365-246X.1970.tb06738.x
McLandress C, Ward WE (1994) Tidal/gravity wave interactions and their influence on the large-scale dynamics of the middle atmosphere: model results. J Geophys Res Atmospheres 99(D4):8139–8155
Mitchell NJ et al (2002) Mean winds and tides in the Arctic mesosphere and lower thermosphere. J Geophys Res Space Phys 107(A1):SIA21214. https://doi.org/10.1029/2001ja900127
Oberheide J, Gusev OA (2002) Observation of migrating and nonmigrating diurnal tides in the equatorial lower thermosphere. Geophys Res Lett 29(24):201–204. https://doi.org/10.1029/2002GL016213
Onwumechili CA (1967) Physics of geomagnetic phenomena, 1. Academic Press, New York, pp 425–507. https://doi.org/10.1016/B978-0-12-480301-5.50014-8
Parish HF, Forbes JM, Kamalabadi F (1994) Planetary wave and solar emission signatures in the equatorial electrojet. J Geophys Res Space Phys 99(A1):355–368. https://doi.org/10.1029/93JA02096
Rastogi RG, Iyer KN (1976) Quiet day variation of geomagnetic H-field at low latitudes. J Geomagn Geoelectr 28(6):461–479. https://doi.org/10.5636/jgg.28.461
Richards PG, Fennelly JA, Torr DG (1994) EUVAC: a solar EUV flux model for aeronomic calculations. J Geophys Res 99:8981–8992
Richmond AD, Matsushita S, Tarpley JD (1976) On the production mechanism of electric currents and fields in the ionosphere. J Geophys Res 81:547–555. https://doi.org/10.1029/JA081i004p00547
Siddiqui TA, Maute A, Pedatella N, Yamazaki Y, Lühr H, Stolle C (2018a) On the variability of the semidiurnal solar and lunar tides of the equatorial electrojet during sudden stratospheric warmings. Ann Geophys 36:1545–1562. https://doi.org/10.5194/angeo-36-1545-2018,2018
Siddiqui TA, Yamazaki Y, Stolle C, Lühr H, Matzka J, Maute A, Pedatella N (2018b) Dependence of lunar tide of the equatorial electrojet on the wintertime polar vortex, solar flux, and QBO. Geophys Res Lett 45(9):3801–3810
Soares G, Yamazaki Y, Matzka J, Pinheiro K, Morschhauser A, Stolle C, Alken P (2018) Equatorial counter electrojet longitudinal and seasonal variability in the American sector. J Geophys Res Space Phys 123:9906–9920. https://doi.org/10.1029/2018JA025968
Soares G, Yamazaki Y, Cnossen I, Matzka J, Pinheiro KJ, Morschhauser A et al (2020) Evolution of the geomagnetic daily variation at Tatuoca, Brazil, from 1957 to 2019: a transition from Sq to EEJ. J Geophys Res Space Phys 125:e2020JA028109. https://doi.org/10.1029/2020JA028109
Soares G, Yamazaki Y, Morschhauser A, Matzka J, Pinheiro KJ, Stolle C et al (2022) Using principal component analysis of satellite and ground magnetic data to model the equatorial electrojet and derive its tidal composition. J Geophys Res Space Phys 127:e2022Ã91
Stening RJ (1969) An assessment of the contributions of various tidal winds to the Sq current system. Planet Space Sci 17(5):889–908. https://doi.org/10.1016/0032-0633(69)90095-6
Sun R, Gu S, Dou X, Li N (2022) Tidal structures in the mesosphere and lower thermosphere and their solar cycle variations. Atmosphere 13:2036. https://doi.org/10.3390/atmos13122036
Takeda M (2002) The correlation between the variation in ionospheric conductivity and that of the geomagnetic Sq field. J Atmos Solar Terr Phys 64(15):1617–1621. https://doi.org/10.1016/S1364-6826(02)00140-2
Takeda M, Maeda H (1980) Three-dimensional structure of ionospheric currents 1. Currents caused by diurnal tidal winds. J Geophys Res Space Phys 85(A12):6895–6899. https://doi.org/10.1029/JA085iA12p06895
Tarpley JD (1970) The ionospheric wind dynamo-I: lunar tide. Planet Space Sci 18(7):1075–1090. https://doi.org/10.1016/0032-0633(70)90109-1
Venkat Ratnam M, Rao VN, Vedavathi C, Murthy KBV (2014) Diurnal tide in the low-latitude troposphere and stratosphere: long-term trends and role of the extended solar minimum. J Atmos Solar Terr Phys 121:168–176. https://doi.org/10.1016/j.jastp.2014.06.004
Wardinski I, Mandea M (2006) Annual and semi-annual variations of the geomagnetic field components analysed by the multi-taper method. Earth Planets Space 58:785–791. https://doi.org/10.1186/BF03351982
Yamazaki Y (2013) Large lunar tidal effects in the equatorial electrojet during northern winter and its relation to stratospheric sudden warming events. J Geophys Res Space Phys 118:7268–7271. https://doi.org/10.1002/2013JA019215
Yamazaki Y, Kosch MJ (2014) Geomagnetic lunar and solar daily variations during the last 100 years. J Geophys Res Space Phys 119(8):6732–6744. https://doi.org/10.1002/2014JA020203

Publisher's Note